Available online at www.sciencedirect.com
ScienceDirect
Journal of the European Ceramic Society 31 (2011) 2711–2719
www.elsevier.com/locate/jeurceramsoc

Influence of intergranular phases on edge integrity of Si_3N_4/SiC wood cutting tools

C. Strehler [a,e,*], M. Parlinska-Wojtan [b], G. Blugan [a], B. Speisser [c], B. Ehrle [d], C.G. Aneziris [e], T. Graule [a,e], J. Kuebler [a]

[a] *Laboratory for High Performance Ceramics, Empa, Swiss Federal Laboratories for Materials Science and Technology, CH-8600 Dübendorf, Switzerland*
[b] *Centre for Electron Microscopy, Empa, Swiss Federal Laboratories for Materials Science and Technology, CH-8600 Dübendorf, Switzerland*
[c] *Ceratizit Luxembourg S. à r.l., L-8201 Mamer, Luxembourg*
[d] *OERTLI Werkzeuge AG, CH-8181 Höri, Switzerland*
[e] *Technical University of Freiberg, Institute of Ceramic, Glass and Construction Materials, D-09599 Freiberg, Germany*

Available online 1 March 2011

Abstract

Si_3N_4/SiC composites used for industrial wood cutting were processed by a near net shape route involving gas pressure sintering with sintering additives such as Al_2O_3, La_2O_3, Y_2O_3 and MgO. The cutting edge integrity of these knives was tested in a cutting trial and compared to knives made by a hot pressing route. It was found that the intergranular phase has a crucial influence on the cutting edge integrity. The boundary phase was analysed by EFTEM and EDX mapping on TEM samples: in gas pressure sintered composites the crystallisation of the apatite $Y_5Si_3O_{12}N$ phase was identified. In the hot pressed composite the boundary phase consisted only of silicates. These composites showed better edge stability than cutting tools with a Y–N-apatite phase. The formation of the type of intergranular phase was found to be determined by the amount of MgO sintering aid and the temperature of the post sintering heat treatment.

Keywords: Cutting tools; Composites; Hot isostatic pressing; Electron microscopy; Grain boundaries

1. Introduction

Industrial wood cutting is a highly demanding and complex process as wood by its nature is inhomogeneous. Beside the lifetime, the surface quality of the wood is an essential characteristic of the cutting tool. For obtaining a nice surface finish the fibres of the wood must be cut through. Otherwise unaesthetic roughness results upon staining of the wood surface. The integrity of the cutting edge is crucial, as chips on the edge of the cutting tool leave their marks as fine lines and are not acceptable for visible timbre constructions such as window frames. Furthermore, no cooling agent can be used as this would impair the surface quality of the wood. Hence a good thermal conductivity of the cutting tools is important in order to conduct the heat away from the cutting tip. Several other properties such as hardness and fracture toughness contribute to the performance of a cutting tool. However, how the material characteristics influence the cutting edge integrity and wear behaviour are not yet fully understood. For currently used tungsten carbide wood cutting tools it is known that their lifetime is limited by abrasive wear and corrosive attack.[1,2]

Si_3N_4 ceramics are low density materials which display high hardness, strength and corrosion resistance. The addition of SiC can give a composite with even higher hardness and better thermal conductivity than intrinsic Si_3N_4. A Si_3N_4/SiC composite is therefore a promising material for wood cutting applications. In a preliminary study Si_3N_4/SiC cutting tools showed 3–4 times longer lifetime than commercial standard tungsten carbide (WC) tools.[3] A mixture of La_2O_3 and Y_2O_3 sintering additives, together with Al_2O_3 from the milling balls were found to give the best combination of properties for wood cutting tools. However, the processing cost for these knives made by hot pressing, diamond cutting and post-hot isostatic pressing were too high

* Corresponding author at: Laboratory for High Performance Ceramics, Empa, Swiss Federal Laboratories for Materials Science and Technology, CH-8600 Dübendorf, Switzerland.

0955-2219/$ – see front matter © 2011 Elsevier Ltd. All rights reserved.
doi:10.1016/j.jeurceramsoc.2011.01.021

for commercial viability. Hence, a near net shape fabrication route was developed, which involved die pressing, gas pressure sintering, diamond finishing and hot isostatic pressing.[4] Due to the lack of mechanical pressure in gas pressure sintering compared to hot pressing the densification is hindered. Hence, the sintering additives necessary for consolidation of the Si_3N_4 composite by liquid phase sintering must be adjusted. For enhancing the densification of liquid phase sintered ceramics there are two approaches: increasing the amount of additives or choose additives which form low viscosity melts, such as MgO. However, MgO is known to negatively influence the mechanical properties of Si_3N_4 ceramics, especially at elevated temperatures.[5] Hence, more refractory sintering additives, such as Y_2O_3 or La_2O_3 are preferred. Rare earth elements such as La_2O_3 or Yb_2O_3 are known to improve the fracture toughness of Si_3N_4 ceramics by promotion of elongated β-Si_3N_4 grain growth.[6] Beside the grain shape, also the chemistry of the interface is crucial for improving the fracture toughness, as only a weak interface allows debonding and makes crack bridging and grain pull out possible.[7] A further improvement of mechanical properties can be achieved by performing a post sintering heat treatment.[8,9] There are several explanations existing for the positive effect of such heat treatments on the mechanical properties. The first suggests that due to the differences in thermal expansion coefficients between the crystallising multiple grain junctions, the amorphous grain boundary phase and the matrix grains, additional stresses are induced, which then facilitate the interfacial debonding and crack deflection.[10,11] The second explanation suggests that the bonding characteristics of the thin grain boundary film are crucial for the strength and fracture toughness improvement.[12,13] Additionally a partially crystalline phase compared to an amorphous phase may have better intrinsic properties. Also for wood cutting applications it was shown that a post-HIP treatment is indispensable as it increases the cutting edge integrity and the cutting performance. Furthermore, it was shown that tools produced by hot pressing have better edge integrity than tools made by gas pressure sintering.[4]

The objective of this study is to identify the most important parameters which are responsible for governing the cutting performance and edge integrity of the Si_3N_4/SiC wood cutting tools. The microstructural and mechanical properties such as: hardness, indentation fracture toughness and edge toughness were investigated. A particular interest was focussed on the composition of the intergranular phase determined by analytical TEM and XRD. Moreover, the evolution of the intergranular phase as a function of the MgO content and of the hot isostatic pressing temperature was studied by XRD.

2. Experimental

The Si_3N_4/SiC composites were synthesised from commercially available Si_3N_4 grade M11 and SiC grade UF25 (both H.C. Starck, Germany). The sintering additives were Al_2O_3 (CT3000, Alcoa, Germany), $La(OH)_3$ (99.9% Auer-Remy GmbH, Germany), $MgCO_3$ (pentahydrate, H.C. Starck, Germany) and Y_2O_3 (grade C, H.C. Starck). Composite named H was prepared by hot-pressing at 1800 °C and 30 MPa uniaxial pressure in nitrogen atmosphere, for further processing details see Eblagon et al.[3] Composites abbreviated with G were densified by a two step gas pressure sintering cycle at 10 and 70 bar at a maximum temperature of 1860 °C. Further details about the processing are given in a previous publication.[4] The exact composition and abbreviation of the specimens described in this work are given in Table 1. The first numbers give the total amount of Al_2O_3, La_2O_3 and Y_2O_3 sintering additives in weight percent, while the second number is the quantity of MgO (wt%) added to the composite. A post sintering treatment was performed on all specimens by hot isostatic pressing (HIP) at 1950 bar nitrogen pressure for 4 h. The HIP temperature was varied between 1200 °C and 1500 °C.

Table 1
Detailed composition of investigated specimen. Mechanical and microstructural investigations, as well as cutting trials were carried out with specimen H, G5.9+2 and G12. Composites G5.9+2, G8+2 and G9+1 were used for investigating the phase evolution as a function of the MgO content.

	H	G5.9+2	G12	G8+2	G9+1
Si_3N_4 (wt%)	65.0	65.0	63.2	62.6	62.6
SiC (wt%)	27.0	27.0	27.8	27.3	27.3
Al_2O_3 (wt%)	0.9	1.1	2.2	1.6	1.8
Y_2O_3 (wt%)	2.3	2.3	4.3	3.1	3.5
La_2O_3 (wt%)	4.7	2.5	5.5	3.4	3.8
MgO (wt%)	–	2.1	–	2.0	1.0

The intergranular phase was analysed by long time X-ray diffraction (XRD) (Pananalytic XiPert Pro, Phillips) using a Cu Kα source. It was carried out on polished bulk specimens with a scan time of 0.5 min/step and a step size of 0.005° from 2θ angles of 10–80°. The structure and the intergranular phase of specimens H and G5.9+2 were analysed in detail by transmission electron microscopy (TEM), energy filtered TEM (EFTEM) and energy dispersive X-ray diffraction (EDX). An overview of the microstructure was performed on a CM30 (Phillips) with a LaB_6 electron gun operating at 300 kV. The analytical TEM analysis was carried out on a 2200FS TEM/STEM (JEOL, Japan) equipped with an omega filter and a Schottkey field emission gun operating at 200 kV. The specimens were mechanically polished down to a few microns thickness using a tripod holder and then argon ion milled to electron transparency.

In order to observe the crack propagation path in the Si_3N_4/SiC composites by SEM (Hitachi S-4800, Japan) a Vickers indenter (2 kg load) was loaded on polished specimens, leading to radial cracking. For revealing the microstructure the specimens were subsequently etched in CF_4/O_2 plasma (RIE 80+, Oxford Instruments, UK). The Vickers hardness was determined according to the procedure EN 843-4.[14] Both Vickers hardness and indentation fracture resistance were evaluated at a load of 2 kg with a dwell time of 15 s. For the hot pressed specimens the hardness, fracture toughness as well as the microstructure was analysed parallel to the pressing direction. The lengths of the indented diagonals and the sizes of the surface cracks were measured with a light microscope (Leitz Wetzlar Durimet, Germany) immediately after the unloading. The indentation fracture resistance was calculated using Miyoshi's equation according to the Japanese Industrial Standard.[15] The

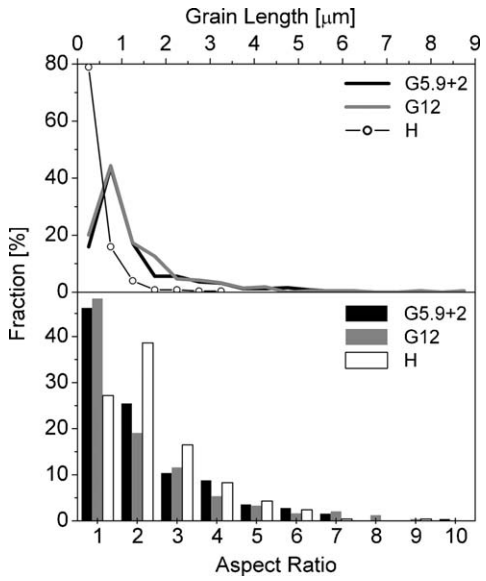

Fig. 1. Aspect ratio of β-Si_3N_4 grains and grain length distribution for composite H, G5.9+2 and G12.

edge toughness test was performed according to the procedure described in CEN 823.[16] A Rockwell indenter was placed close to the 90° edge the specimens. A constantly increasing load was applied (Zwick Z005, Germany) until flaking of the edge occurred. The ratio of the flaking load and the thickness of the chip is termed edge toughness. Chips of various thickness were produced, the average edge toughness and the standard deviation was calculated. The density was determined using the Archimedes principle. The theoretical density was calculated from the composition of the specimen using the rule of mixture.

The cutting trials for tools H, G5.9+2 and G12 were performed on a moulding machine (Type HAC, GF Brugg, Switzerland) with laminated glued beech having cross fibred and longitudinal sections. The rotation speed was set to 8000 rpm, the feed of the wood plank was 12 m/min and the cutting depth 5 mm. The surface quality of the wood was evaluated by an experienced carpenter with an empirical roughness test by hand. Short-term cutting trials (2 m) were performed only in order to test the first-cut quality and the edge integrity of the tools.

3. Results and discussion

3.1. Mechanical properties and microstructure

Table 2 gives the HIP temperature and a summary of microstructural and mechanical properties of composites H, G5.9+2 and G12. A HIP temperature of 1400 °C instead of 1200 °C was chosen for composite G12, as the experiments described in the next paragraphs of this paper show that a higher HIP temperature is more beneficial for the crystallisation of the intergranular phase. The density for composite H is around 99% and 97.5% for composite processed by gas pressure sintering. Eblagon et al. showed that the density is a crucial factor for the cutting performance.[3] Pores can act as origins for chipping and may reduce the edge integrity and hence the cutting quality.

The hardness is known to be important for the wear behaviour of a cutting tool.[17] The Vickers hardness was measured to be slightly higher for the hot pressed composite H (18.25 GPa) compared to the gas pressure sintered specimens G5.9+2 (16.57 GPa) and G12 (16.4 GPa), which are typical values for this type of composites found in literature.[18,19] The indentation fracture

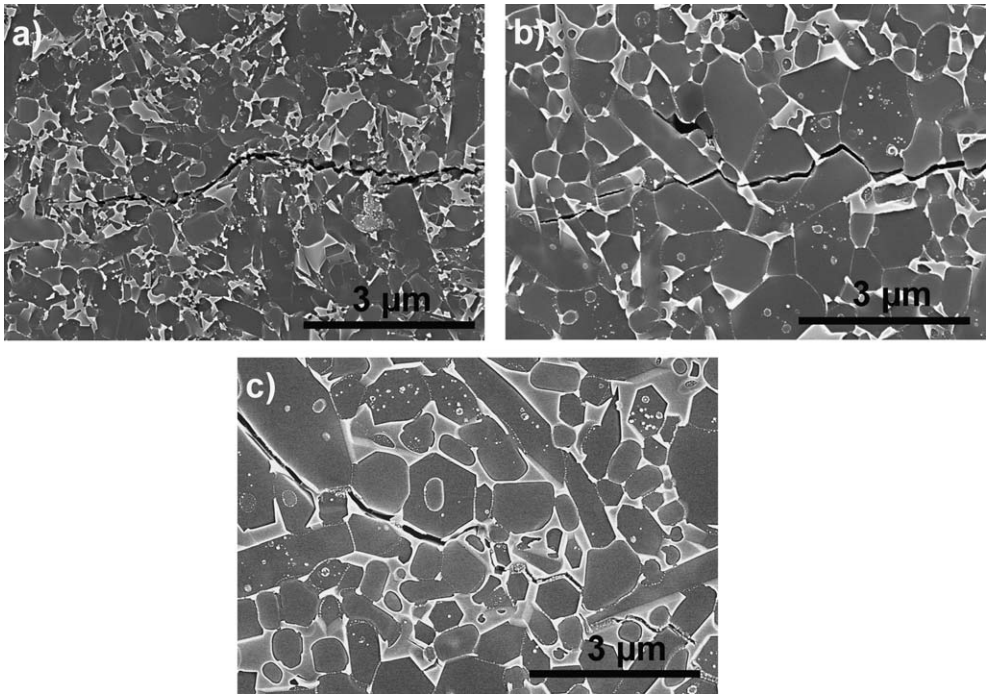

Fig. 2. SEM images showing the microstructure and the crack propagation path of specimens H (a), G5.9+2, (b) and G12 (c). The cracks originate from the corners of a Vickers indent. Specimen G12 shows less transgranular fracture than composites H and G5.9+2.

Table 2
Detailed composition of investigated specimen. Mechanical and microstructural investigations, as well as cutting trials were carried out with specimen H, G5.9+2 and G12. Composites G5.9+2, G8+2 and G9+1 were used for investigating the phase evolution as a function of the MgO content.

	H	G5.9+2	G12
HIP temperature (°C)	1200	1200	1400
Density (%)	99.5 ± 0.2	97.5 ± 0.3	97.4 ± 0.4
Average grain size (μm)	0.35 ± 0.09	0.72 ± 0.18	1.02 ± 0.18
Vickers hardness (GPa)	18.25 ± 0.58	16.57 ± 0.20	16.4 ± 0.56
Indentation fracture resistance (MPa m$^{1/2}$)	5.85 ± 0.4	5.24 ± 0.29	5.4 ± 0.22
Edge toughness (N/mm)	530 ± 50	496 ± 44	509 ± 36
First cutting quality	Good	Not acceptable	Good

Table 3
Intergranular phase formed in different compositions with different MgO content and at various HIP temperatures. X: unidentified phase.

	G5.9+2	G8+2	G9+1
1200 °C	$Y_5Si_3O_{12}N$	$Y_5Si_3O_{12}N + X$	$Y_5Si_3O_{12}N$
1300 °C	$Y_5Si_3O_{12}N + X$	$Y_5Si_3O_{12}N + X$	$Y_5Si_3O_{12}N$
1400 °C	$Y_5Si_3O_{12}N$	$Y_2Si_2O_7$	$Y_5Si_3O_{12}N + Y_2Si_2O_7$
1500 °C	–	–	$Y_2Si_2O_7$

toughness with values around 5.5 MPa$\sqrt{}$m and the edge toughness are in the same range for all three composites, independent of the processing route and the additive system. Si_3N_4/SiC composites, with similar parameters to the ones studied in this paper were produced by Lee following a reaction bonding and gas pressure sintering route with Al_2O_3 and Y_2O_3 sintering aids.[18] They exhibited a hardness of 16.8 GPa and an indentation fracture toughness of 5.2 MPa$\sqrt{}$m. In fully dense Si_3N_4/SiC composites made by GPS with Y_2O_3 sintering aid Herrmann et al. measured. A Vickers hardness HV10 of 16.8 GPa and an indentation fracture toughness of 4.1 MPa$\sqrt{}$m.[19]

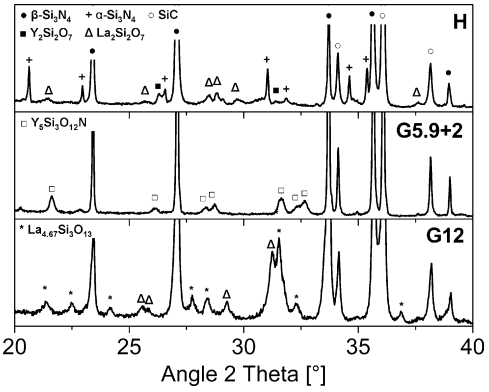

Fig. 3. XRD-spectra of composite H, G5.9+2 and G12.

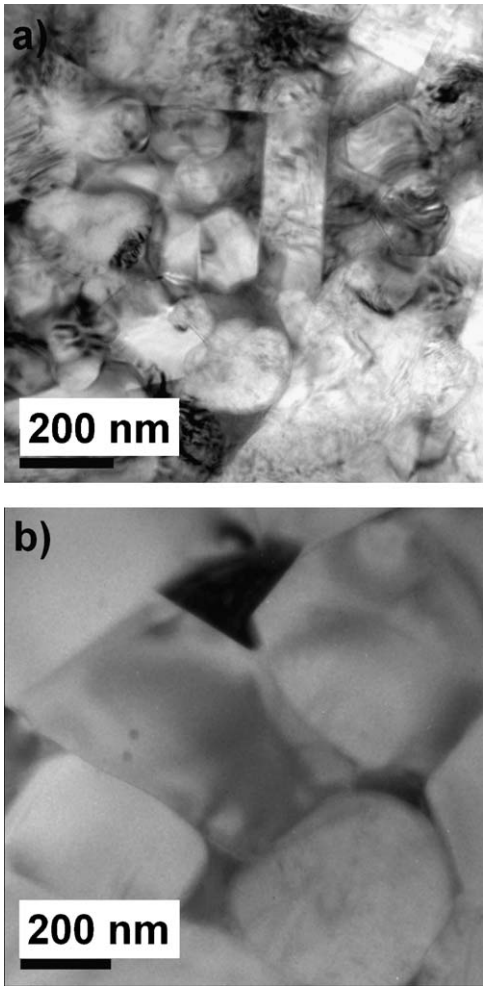

Fig. 4. TEM bright field images showing the typical microstructure of composite H (a) and G5.9+2 (b).

The differences in processing route are clearly visible in the microstructure: the grain size (Table 2) of the hot pressed composite (0.34 μm) is smaller than the one of the near net shape processed composites (0.72–1.02 μm). This fact was previously observed by the authors[4] and is due firstly to the shorter process time in hot pressing, which allows less time for grain growth and secondly to the mechanical pressure counteracting the grain growth. Composite G12 has larger grains than G5.9+2, which is due to the higher quantity of sintering additives. Fig. 1 shows the aspect ratio and the grain size distribution. Composite H has more elongated grains than the gas pressure sintered specimens. This can be explained by the uniaxial mechanical pressure applied in hot pressing. The SEM images in Fig. 2 show the microstructures of composites H, G5.9+2 and G12, together with the crack propagation path. A combination of trans- and intergranular fracture is seen for all specimens. However, composite G12 shows less transgranular fracture than tool H and G5.9+2. Intergranular fracture behaviour and elongated Si_3N_4 grains are desired, as they are necessary for obtaining high fracture toughness. This type of microstructure allows the dissipation of energy by mechanisms such as crack deflection and crack bridging. It is known from literature,[20,21] that the fracture toughness increases

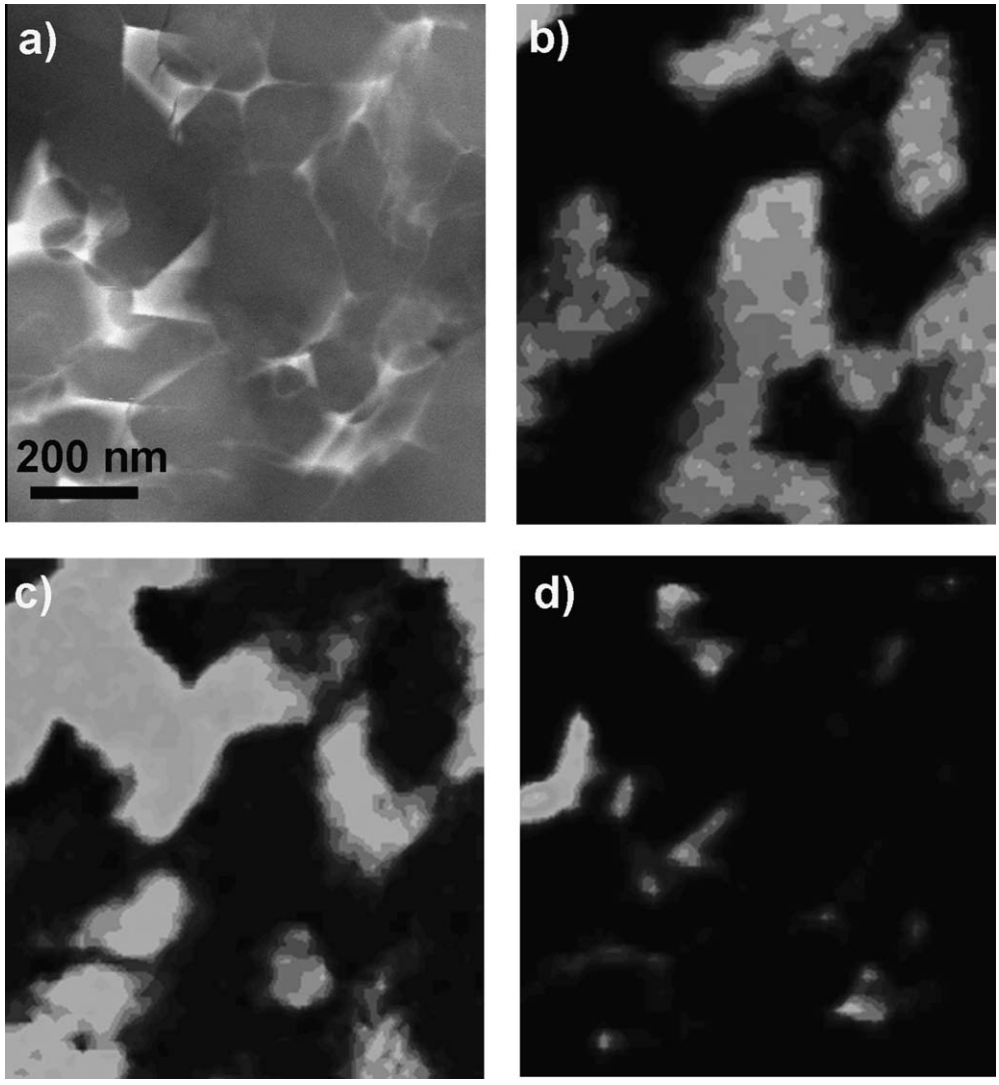

Fig. 5. STEM image of composite H (a). Elemental map of C (light) identifying the SiC grains (b) and N-map in light (c) giving the location of the Si_3N_4 grains. The intergranular phase is shown by the La-map in light (d). Comparison of (c) and (d) shows that no N is found in the intergranular phase.

with increasing grain size and increasing aspect ratio. Consequently, composite H with its more elongated grains, compared to the ones in composite G5.9+2 and G12, should yield a higher fracture resistance. Unfortunately the smaller grain size counteracts this effect. Beside the aspect ratio and the grain size, it is well known that the chemistry and crystallinity of the intergranular phase play a crucial role in governing mechanical properties.[7] XRD diffractogramms of composite H, G5.9+2 and G12, shown in Fig. 3, reveal clear differences in the intergranular phases after HIP at 1200 °C (tool H and G5.9+2) and 1400 °C (tool G12). Sample H made by hot pressing shows $Y_2Si_2O_7$ and $La_2Si_2O_7$ phases, while composite G5.9+2 prepared by GPS with MgO addition displays an apatite-like phase ($Y_5Si_3O_{12}N$). Composite G12 exhibits only the $La_{4.67}Si_3O_{13}$ phase.

3.2. TEM-analysis of the intergranular phase

The TEM investigations of composite H and G5.9+2 were performed in order to analyse the structural and chemical composition of the intergranular phase. The TEM images in Fig. 4 show a typical microstructure of samples G5.9+2 and H, showing a finer microstructure of specimen H. EDX maps in STEM mode of the distribution of the C, N and La in composite H are depicted in Fig. 5. This allows the differentiation between Si_3N_4, SiC grains and the intergranular phase. Besides La, the elements Y and O were also detected in the intergranular phase. This is in accordance with the XRD results, where silicon oxide phases were measured. An elemental mapping of composite G5.9+2 by energy filtered TEM (EFTEM) allowed the identification of SiC, Si_3N_4 grains and of the intergranular phase (Fig. 6). Further, the EFTEM maps show that the multiple grain pockets of specimen G5.9+2 are composed of Y, La, Mg and O. Al could not be detected by energy filtered TEM, due to the fact that the energy loss values of Al are in energy ranges, which are difficult to detect. An EDX-linescan across the intergranular phase shows the presence of the sintering elements such as: Y, La, Mg and O (Fig. 7b), confirming the results obtained by EFTEM mapping. Furthermore, with the EDX mapping, Al could be detected at

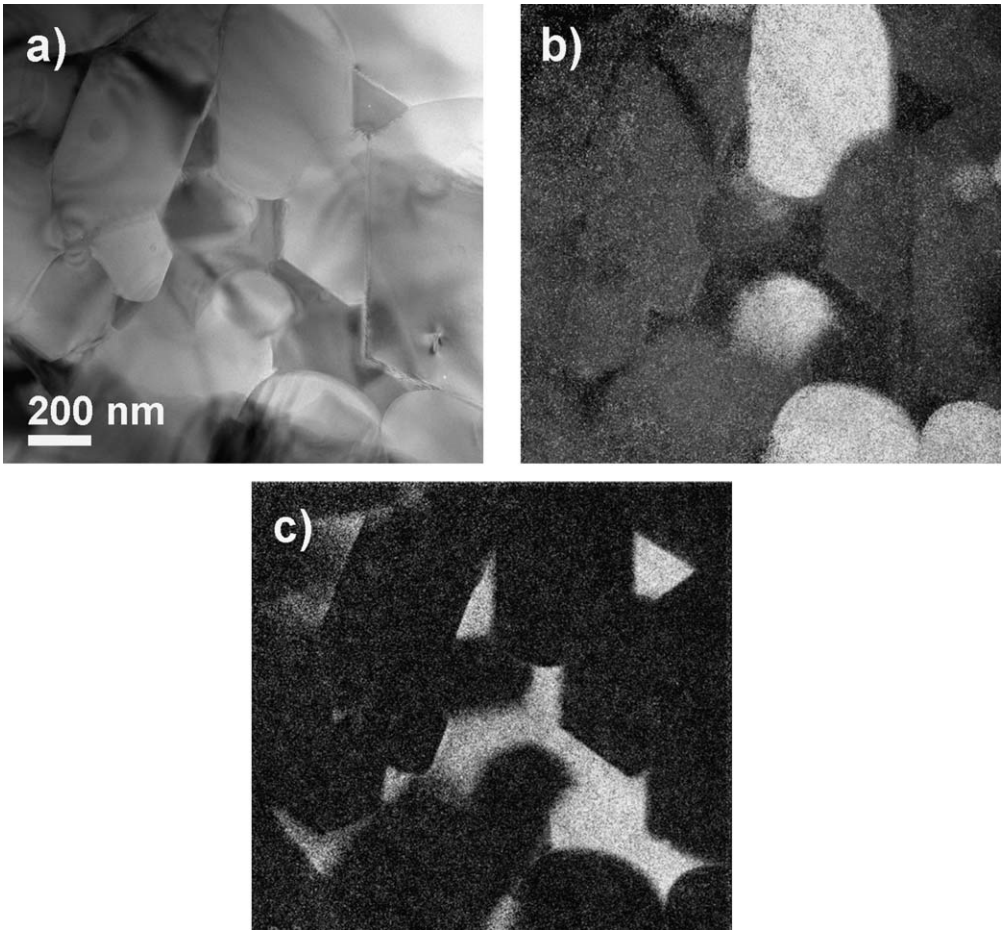

Fig. 6. EFTEM images of composite G5.9+2: TEM bright field image of the analysed area (a), overlay of Si-map (grey) and C-map (light) showing the Si_3N_4 and SiC grains (b). Overlay of La-, Y-, Mg- and O-maps in light, these elements are all located in the intergranular phase.

the borders of the intergranular phase (Fig. 7d). It seems that the crystallisation of the intergranular phase leads to a depletion of Al. Hence, Al is pushed to the borders of the multigrain pockets. A depletion of the multiple grain junctions and a subsequent enrichment of residual glass phase with Al were described by Bodur et al. for Si_3N_4 densified with Y_2O_3 and Al_2O_3.[22] Moreover, the STEM-EDX mapping of nitrogen shows that N is not only found in the Si_3N_4 grains, but that it is also present in the intergranular phase. This confirms the XRD spectrum, where the crystalline phase was identified as $Y_5Si_3O_{12}N$. This is in contrast to composite H, were no N was identified in the intergranular phase.

3.3. Cutting trial and edge integrity

The qualitative results of the short-term cutting trial, determined as described by an empirical test, are given in Table 2. Cutting tools H and G12 give a good first-cut surface quality, while tool G5.9+2 showed chipping, which results in an unacceptable quality of the cut wood surface. The cutting edge of tool G5.9+2 and the corresponding wood surface is shown in Fig. 8. Chipping only occurs in the area where the tool cuts the hard sections of the beech composed of cross grained wood with high glue content. The chipping of the cutting edge leads to a blunting and proper cutting through of the wood fibres becomes impossible. Hence, the resulting wood surface is very rough and the cutting quality is unacceptable.

Several mechanical and materials properties such as hardness and fracture toughness contribute to the performance of a cutting tool. However, how the materials characteristics influence the cutting edge integrity and wear behaviour are not clearly understood. Density, hardness, indentation fracture toughness and edge toughness, which give the macroscopic properties of a material, are not sufficient to explain the quality of the wood cutting tool edge. The first cut quality of the two gas pressure sintered tools is different, even though there is no significant difference in mechanical properties that were measured. According to the experiments the intergranular phase is playing a critical role in determining the edge integrity. Silicon oxide phases, as developed in tool H and G12, are the preferred phases for cutting applications. The edge integrity of Si_3N_4/SiC composite G5.9+2 with $Y_5Si_3O_{12}N$ phase is unacceptable. Apatite-like phases, i.e. $Y_5Si_3O_{12}N$, have a coefficient of thermal expansion of about

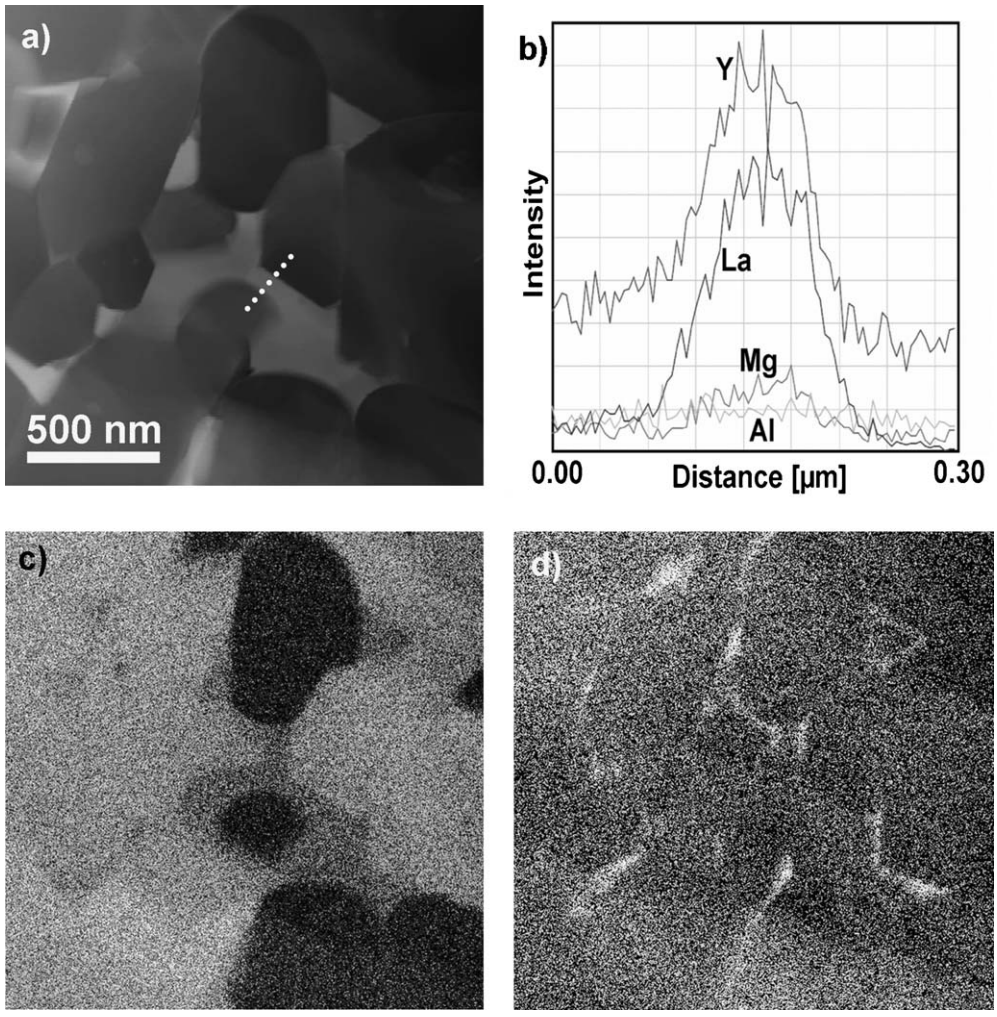

Fig. 7. (a) STEM image of tool G5.9+2: image of the analysed area acquired with the HAADF detector (a). EDX scan along the line marked in (a) confirming the presence of Y, La and Mg in the intergranular phase (b). N-map (light) showing that N is also found in the intergranular phase (c). Map of Al (light) which is pushed to the borders of the intergranular phase (d).

$10^{-5}\,K^{-1}$,[23] which is higher compared to e.g. $\sim 3.9\,10^{-6}$ for $Y_2Si_2O_7$.[24] Lojanova et al. suggest that due to the difference of thermal expansion coefficient between the apatite-like phase located in the triple points and Si_3N_4 significant local stresses are induced, which negatively influence the fracture behaviour of ceramics with apatite-like phases.[23] The crack path analysis shows that there is a difference in microscopic fracture behaviour. Composite G12 shows less transgranular fracture than specimen G5.9+2. Although this fact is not reflected in the indentation fracture toughness or in the edge chipping measurements, it could play an important role in determining the edge integrity. It was further stated that $Y_2/La_2Si_2O_7$ in contrast to apatite-like phases has the higher oxidation resistance and is better for high temperature mechanical properties of Si_3N_4 ceramics.[25] However, we assume that for short-term cutting tests the issue of corrosion and excessive temperature can be neglected.

3.4. Evolution of the intergranular phase

A series of HIP treatments, at 1200–1500 °C were performed with compositions G5.9+2, G8+2 and G9+1. The intergranular phases generated after every treatment are listed in Table 3. The apatite-like phase $Y_5Si_3O_{12}N$ was preferentially formed at lower heat treatment temperature, while the yttrium disilicate phase starts to form at 1400 °C and higher. In composite G5.9+2 the $Y_2Si_2O_7$ phase does not form at all. However, it forms in specimens G8+2 and G9+1. Hence, it forms in composites which have a lower amount of MgO compared to the total amount of additives. MgO tends to hinder the crystallisation of $Y_2Si_2O_7$ and $La_2Si_2O_7$. From the analytical TEM analysis it is known, that the MgO is homogeneously distributed in the intergranular phase of tool G5.9+2 thus holding an interstitial position in the crystalline $Y_5Si_3O_{12}N$ pockets. A similar observation was made by Becher et al. who observed the crys-

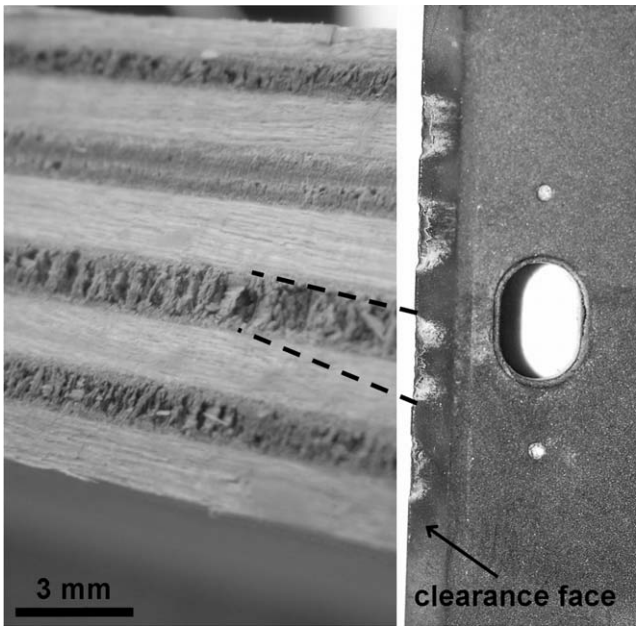

Fig. 8. Unacceptable roughness of the wood surface (left) cut with tool G5.9+2 (right). Chipping takes place where the tool cuts the hard sections of the wood containing cross fibred wood with high glue content (dashed lines). Residues of glue are visible on the clearance face of the tool.

tallisation of the $La_{4.67}Si_3O_{13}$ phase in Si_3N_4 specimens with La_2O_3 and SiO_2 sintering aids.[26,27] However, for specimens densified with La_2O_3 and MgO additives the nitrogen containing phase of $LaSiO_2N$ was detected.

4. Conclusions

The influence of mechanical and microstructural properties on the integrity of the cutting edges of wood cutting tools made of Si_3N_4/SiC composites with sintering additives such as Al_2O_3, La_2O_3, Y_2O_3 and MgO were investigated during real cutting trials on wood. The hardness and fracture toughness values for all composites, independently on the sintering additives and the processing method by hot pressing or gas pressure sintering, were varying between 16–18 GPa and 5.2–5.85 $MPa\sqrt{m}$, respectively. Thus, it seems that macroscopic mechanical properties such as hardness, indentation fracture resistance or edge toughness cannot be used as measures for the performance of a wood cutting tool. However, TEM observations revealed clear differences in the microstructures: the grain size of the hot pressed composites was about 0.34 μm, contrary to the neat net shape processed composites with grain sizes varying from 0.72 μm to 1 μm. Moreover, the most important parameter playing a crucial role in determining the cutting edge integrity was the intergranular phase, which was analysed by TEM and XRD. Si_3N_4/SiC cutting tools without MgO sintering aid display a La/Y-silicon oxide phase and show superior edge integrity. They are preferred over cutting tools with MgO addition which have an apatite-like phase ($Y_5Si_3O_{12}N$). Simultaneously, the crystallisation of the apatite-like phase leads to the depletion of Al from this phase, which is thus located at the edges of the intergranular pockets. Heat treatments of the composites at 1200 °C and 1500 °C allowed finding out that MgO is an undesired sintering additive, and that it hinders the crystallisation of the silicon–oxide phase, which is beneficial for the edge integrity of the wood cutting tools.

Acknowledgements

We would like to thank H. Hank and M. Hellstern from Ceratizit Horb GmbH for the diamond machining of the composite knives. We acknowledge the support of P. Burkard from the FIRST Lab at ETH Zürich who helped with the plasma etching of the specimens. This work was funded by the Swiss Commission for Technology and Innovation (CTI) under the grant No. 8989.1PFIW-IW.

References

1. Sheikh-Ahmad JY, Bailey JA. The wear characteristics of some cemented tungsten carbides in machining particleboard. *Wear* 1999;**225–229**:256–66.
2. Gauvent M, Rocca E, Meausoone PJ, Brenont P. Corrosion of materials used as cutting tools of wood. *Wear* 2006;**261**:1051–5.
3. Eblagon F, Ehrele B, Graule T, Kuebler J. Development of silicon nitride/silicon carbide composites for wood-cutting tools. *J Eur Ceram Soc* 2007;**27**:419–28.
4. Strehler C, Blugan G, Ehrle B, Speisser B, Graule T, Kuebler J. Influence of sintering and sintering additives on the mechanical and microstructural characteristics of Si_3N_4/SiC wood cutting tools. *J Eur Ceram* 2010;**30**:2109–15.
5. Ziegler G, Heinrich J, Wötting G. Review: relationship between processing, microstructure and properties of dense and reaction-bonded silicon nitride. *Mater Sci* 1987;**22**:3041–86.
6. Becher PF, Sun EY, Plucknett KP, Alexander KB, Hsueh C-H, Lin H-T, et al. Microstructural design of silicon nitride with improved fracture toughness: I. Effects of grain shape and size. *J Am Ceram Soc* 1998;**81**:2821–30.
7. Satet RL, Hoffmann MJ. Influence of the rare-earth element on the mechanical properties of RE_2O_3–Mg–bearing silicon nitride. *J Am Ceram Soc* 2005;**88**:2485–90.
8. Cinibulk MK, Thomas G, Johnson SM. Grain-boundary-phase crystallization and strength of silicon nitride sintered with a YSiAlON glass. *J Am Ceram Soc* 1990;**73**:1606–12.
9. Bonnell DA, Tien T-Y, Ruhle M. Controlled crystallization of the amorphous phase in silicon nitride ceramics. *J Am Ceram Soc* 1987;**70**:460–5.
10. Peterson IM, Tien T-Y. Effect of the grain boundary thermal expansion coefficient on the fracture toughenss of silicon nitride. *J Am Ceram Soc* 1995;**78**:2345–52.
11. Kessler H, Kleebe H-J, Cannon RW, Pompe W. Influence of internal stresses on crystallization of intergranular phases in ceramics. *Acta Metall Mater* 1992;**40**:2233–45.
12. Wötting G, Ziegler G. Influence of powder properties and processing conditions on microstructure and mechanical properties of sintered Si_3N_4. *Ceram Int* 1984;**10**:18–22.
13. Becher PF, Painter GS, Sun EY, Hsueh CH, Lance MJ. The importance of amorphous intergranular films in self-reinforced Si_3N_4 ceramics. *Acta Mater* 2000;**48**:4493–9.
14. EN 843-4. Advanced Technical Ceramics – Monolithic Ceramics – Mechanical Properties at Room Temperature. Part 4. Vickers, Knoop and Rockwell Superficial Hardness Tests.
15. Japanese Industrial Standard JIS R 1607. *Testing methods for fracture toughness of high performance ceramics*; 1995.
16. EN 843-9. Advanced Technical Ceramics – Monolithic Ceramics – Mechanical Properties at Room Temperature. Part 9. Method of Test for Edge-Chip Resistance.
17. Scieszka SF. Edge failure as a means of concurrently estimating the abrasion and edge fracture resistance of hard-metals. *Tribol Int* 2005;**38**:834–42.

18. Lee SY. Fabrication of Si_3N_4/SiC composite by reaction-bonding and gas-pressure sintering. *J Am Ceram Soc* 1998;**81**:1262–8.
19. Herrmann M, Schubert C, Rendtel A, Hübner H. Silicon nitride/silicon carbide nanocomposite materials. I. Fabrication and mechanical properties at room temperature. *J Am Ceram Soc* 1998;**81**:1095–108.
20. Kleebe HJ, Pezzotti G, Ziegler G. Microstructural contributions to the fracture resistance of silicon nitride ceramics. In: Hoffmann MJ, Petzow G, editors. *Tailoring of mechanical properties of Si_3N_4 ceramics*. Netherlands: Kluwer Academic Publishers; 1994.
21. De Pablos A, Osendi MI, Miranzo P. Correlation between microstructure and toughness of hot pressed Si_3N_4 ceramics seeded with [beta]-Si_3N_4 particles. *Ceram Int* 2003;**29**:757–64.
22. Bodur CT, Szabó DV, Kromp K. Effects of heat treatments on the microstructure of a yttria/alumina-doped hot-pressed Si_3N_4 ceramic. *J Mater Sci* 1993;**28**:2089–96.
23. Lojanová S, Tatarko P, Chlup Z, Hnatko M, Dusza J, Lences, et al. Rare-earth element doped Si_3N_4/SiC micro/nano-composites-RT and HT mechanical properties. *J Eur Ceram Soc* 2010;**30**:1931–44.
24. Sun ZQ, Zhu XW, Li MS, Zhou YC, Sakka Y. Tailoring texture of γ-$Y_2Si_2O_7$ by strong magnetic field alignment and two-step sintering. *J Am Ceram Soc* 2008;**91**:2521–8.
25. Chen J, Wei PAN, Huang Y. Formation and properties of La–Y–Si–O–N oxynitride glasses. *J Mater Sci Lett* 1997;**16**:1486–8.
26. Becher PF, Painter GS, Shibata N, Waters SB. *J Am Ceram Soc* 2008;**91**:2328–36.
27. Becher PF, Shibata N, Painter GS, Averill F, van Benthem K, Lin H-T, et al. Observations on the influence of secondary Me oxide additives (Me = Si, Al, Mg) on the microstructural evolution and mechanical behavior of silicon nitride ceramics containing RE_2O_3 (RE = La, Gd, Lu). *J Am Ceram Soc* 2010;**93**:570–80.